Final Draft
of the original manuscript:

Zerbst, U.; Stadie-Frohboes, G.; Plonski, T.; Jury, J.:
The problem of adequate yield load solutions in the context of proof tests on a damaged subsea umbilical
In: Engineering Failure Analysis (2008) Elsevier

DOI: 10.1016/j.engfailanal.2008.05.013

THE PROBLEM OF ADEQUATE YIELD LOAD SOLUTIONS IN THE CONTEXT OF PROOF TESTS ON A DAMAGED SUBSEA UMBILICAL

Uwe. Zerbst [a], Gundula Stadie-Frohbös [b], Thomas Plonski [b], Jonathan Jury [c]

[a] GKSS Research Centre, Institute for Materials Research, Materials Mechanics, D-21502 Geesthacht, Germany

[b] Germanischer Lloyd AG, Vorsetzen 35, D-20459 Hamburg, Germany

[c] RiserTec Limited, Arnhall Business Centre, Westhill, Aberdeenshire AB32 6UF, United Kingdom

Key words: umbilical, fracture mechanics, longitudinal crack, yield load

1. BACKGROUND HISTORY

Subsea umbilicals are composite cable and small diameter tubular bundles deployed on the seabed in conjunction with offshore installations for oil or gas exploitation. Their aim is to supply necessary power and control to remote production valves, chokes and control systems. For this purpose umbilicals consist of cores of cables and tubes encapsulated in a polyurethane sheath for protection as schematically illustrated in Figure 1. The tubes contain control fluids. They are loaded by alternating internal pressure. Once an umbilical is installed on the seabed failure-free operation is intended over its whole lifetime (safe-life design philosophy).

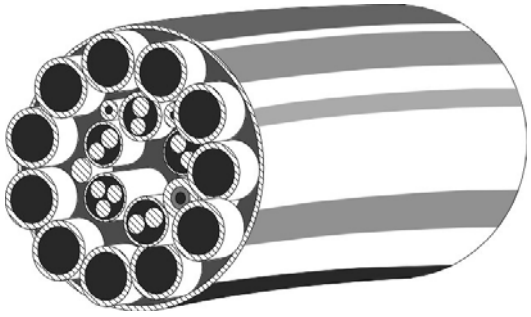

Figure 1: Schematic drawing of the umbilical investigated

In the present case a performance check of the installed umbilical revealed that one tube had a leak and was not able to carry load. In order to find the reason a spare line section was investigated which had experienced the same treatment during manufacture. It was found that some of the tubes were largely ovalised to an extent of 55%. The same section was then used to determine the pressure needed for re-rounding the ovalised pipes. Subsequently this pressure was applied to the installed umbilical as well.

Since it could not be excluded that potential cracks just small enough not to snap through the wall existed in the re-rounded umbilical fracture mechanics investigations were necessary in addition to the confirmation of leak tightness. The general scheme of such an investigation follows a proof test philosophy [1] where the overload test provides information on the

serviceability at the time of the test but not on potential pre-damage which could affect the future component behaviour.
The aim of the fracture mechanics analysis is to provide information on

(a) the maximum crack size in the component which just would not have caused component failure due to the boost pressure applied for re-rounding and on

(b) the residual lifetime of the component under regular in-service loading. This is based on the assumption that the maximum possible crack size at the end of the proof test really exists.

In the present analysis step (b) is further complicated by the fact that the re-rounding process introduces high residual stresses which effect both fatigue crack propagation and final failure.

2. FRACTURE MECHANICS MODELLING

2.1 The Tube Investigated

The tube had an outer diameter of 22 mm and a wall thickness of 1.1 mm. It was made of SAF 2507, a high-alloy super duplex stainless steel. Its tensile properties provided by individual testing (mean value of 6 tests) were:

- Yield strength: 756 MPa,

- Tensile strength: 947 MPa,

- Elongation: 31 %,

and its fracture and crack propagation properties were:

- Crack Tip Opening Displacement: 0.46 mm (maximum of welded SAF 2507)

- Paris parameters of fatigue crack propagation:
  - $C = 2.3 \cdot 10^{-10}$ (mean + 2 standard deviations; for da/dN in mm/cycle and ΔK in $MPa \cdot m^{1/2}$);
  - $m = 3.52$

- Fatigue crack growth threshold $\Delta K_{th} = 6.8\ MPa \cdot m^{1/2}$

(all fatigue data for for R = 0.1 and a frequency of 10Hz)

[6]. The upper service pressure p_{max} of the loading cycle was 34.4 MPa, the lower pressure p_{min} = 2.8 MPa (static head pressure), the boost pressure for re-rounding the tubes was p_{proof} = 65.5 MPa.

2.2 Maximum Potential Crack Size Subsequent To Proof Testing

The fracture mechanics analysis can be carried out completely numerically or by means of analytical assessment procedures such as R6 [2], BS 7910 [3] or SINTAP [4]. Note that the latter has been extended in the European Fitness-for-Service Network (FITNET) recently [5]. These procedures are equivalent with respect to their basic approach. For a detailed introduction into the methodology see [6].

The required input information and the analysis steps of the analytical approach are illustrated in Figure 2. In the following only what is called the FAD method shall briefly be introduced. In the FAD (Failure Assessment Diagram) the crack driving force in terms of the linear elastic stress intensity factor (K factor) is referred to the toughness of the material, K_{mat} (in general terms)

$$K_r = K/K_{mat} \tag{1}$$

and plotted against a ligament yielding parameter L_r defined by

$$L_r = F/F_Y = \sigma_{ref}/\sigma_Y \tag{2}$$

(Figure 3) with F being the load (in general terms), F_Y the yield (or limit) load of the component with crack, σ_{ref} a net section reference stress and σ_Y the yield strength of the material. The FAD curve is defined by

$$K_r = f(L_r) \tag{3}$$

with L_r being a function of the stress-strain curve of the material

$$K_r = f(L_r) = \begin{cases} \left[\dfrac{E \cdot \varepsilon_{ref}}{\sigma_{ref}} + \dfrac{1}{2} \dfrac{L_r^2}{E \cdot \varepsilon_{ref}/\sigma_{ref}} \right]^{-1/2} & \text{for } L_r \le L_r^{max} \\ 0 & \text{for } L_r > L_r^{max} \end{cases} \tag{4}$$

but being independent of the component and loading geometry. L_r^{max} defines the limit condition for plastic collapse failure and is given by:

$$L_r^{max} = 0.5 \cdot \left[(\sigma_Y + R_m)/R_{eL} \right]. \tag{5}$$

The principle of how these equations are used is illustrated in Figure 4. For a given applied load F the ligament yielding parameter L_r in the component is determined by $L_r = F/F_Y$. This is taken as the input parameter for determining a reference stress σ_{ref} by

$$\sigma_{ref} = L_r \cdot \sigma_Y \tag{6}$$

which then defines a corresponding reference strain ε_{ref} on the true stress-stain curve.

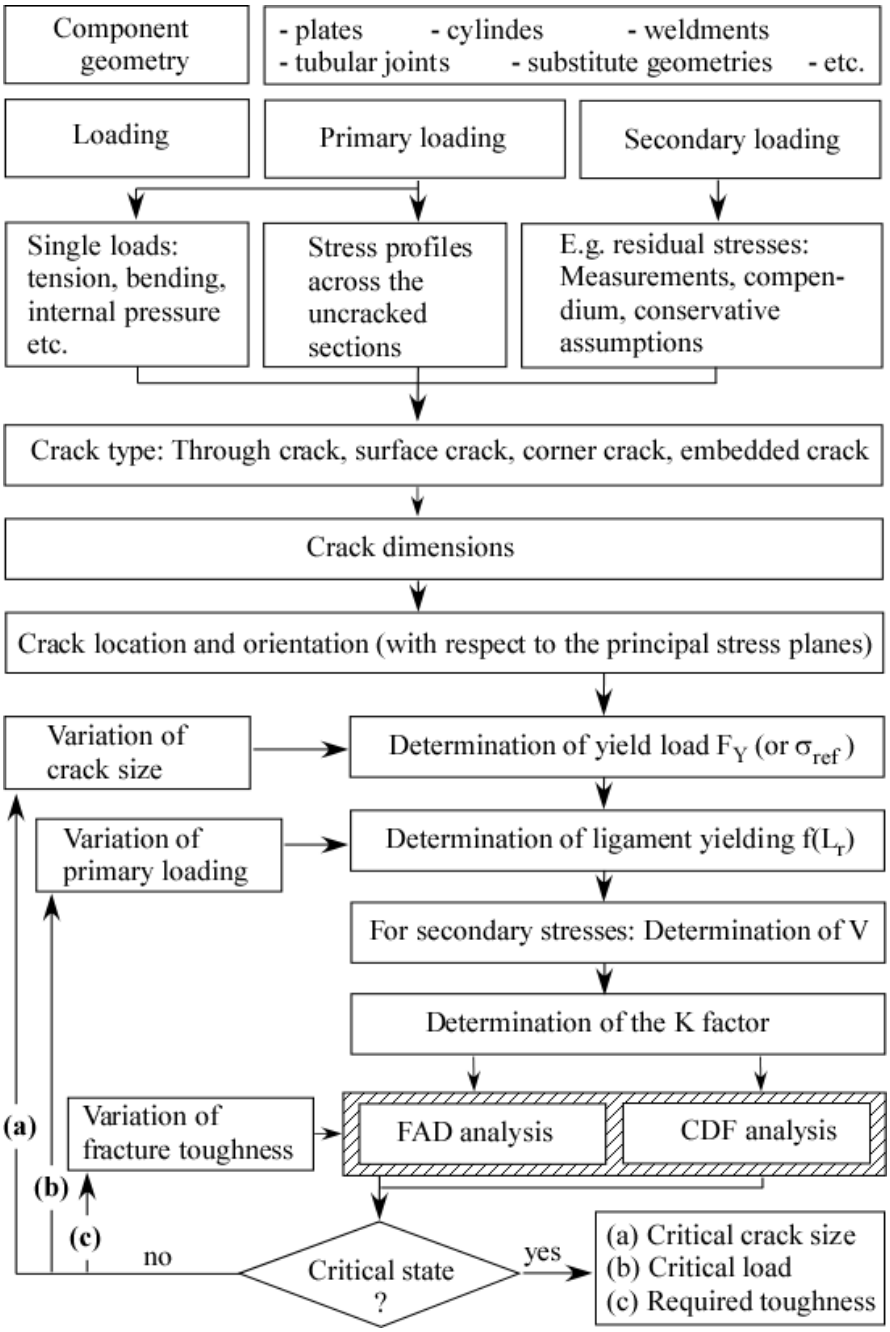

Figure 2: Flow chart of analytical flaw assessment analyses. (a) Determination of critical crack size; (b) Determination of critical load; (c) Determination of minimum required fracture toughness (according to [6]).

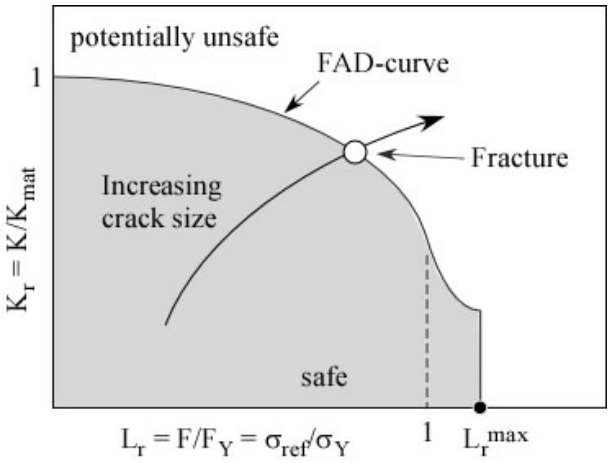

Figure 3: Determination of the critical crack size by the FAD approach.

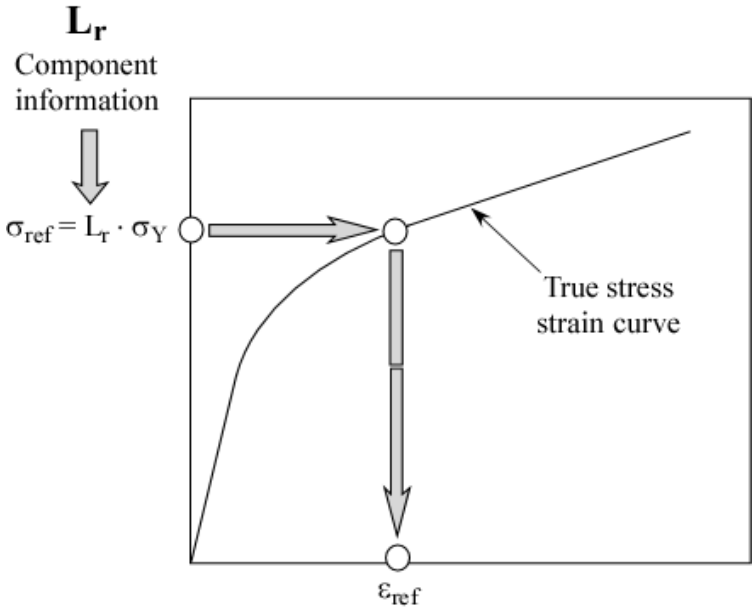

Figure 4: Determination of (σ_{ref},ε_{ref}) points on the true stress-strain curve dependent on the ligament yielding parameter L_r of the component.

Note that the yield load F_Y or the associated reference stress σ_{ref} is a crucial parameter for any assessment since the quality of the whole analysis strongly depends on it. In the present analysis the existence of an internal semi-elliptical axial crack was assumed in a representative tube section. For this case various yield load solutions are available in the literature some of which have been incorporated into compendia of the procedures mentioned above. Most of the solutions have been developed recently. Figure 5 gives an impression of the different crack size dependency of these solutions for crack geometries a/c of 0.05, 0.2 and 1 (a = crack depth; c = half crack length at surface of the semi-elliptical crack).

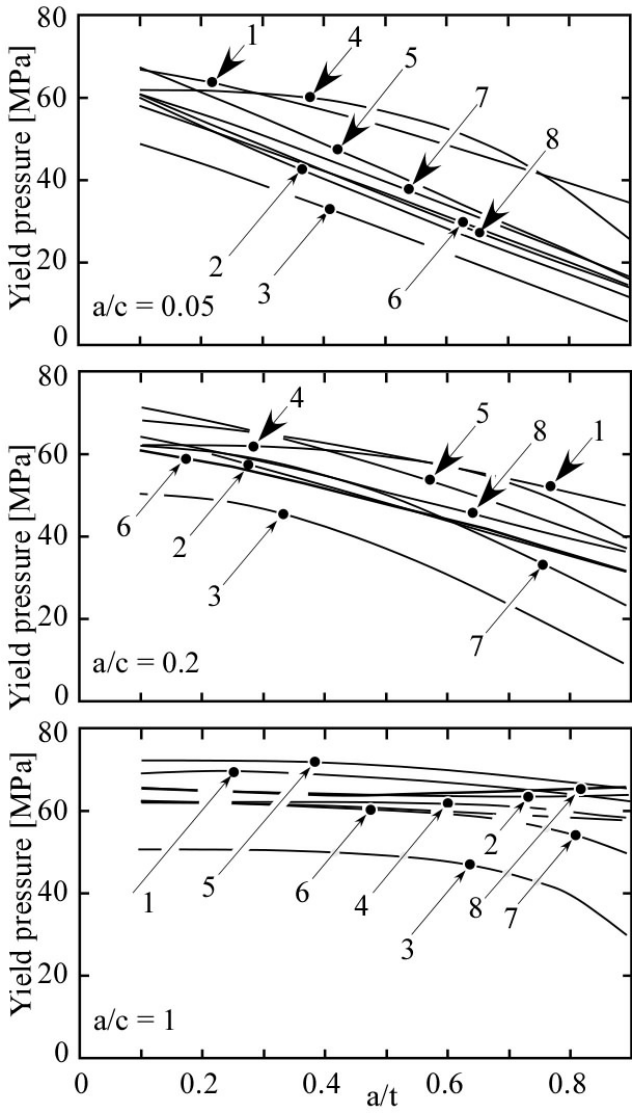

Figure 5: Dependency of various yield load solutions on crack depth referred to wall thickness, a/t, for the material described in Section 3.1 and crack grometries a/c = 0.05, 0.2 and 1: (1) Kim & Shim (2005) [8], (2) R6, Rev. 4 (2001) [2] , (3) BS 7910 (2005) [3], (4) Sattari-Far & Dillström (2004) [9], (5) Staat & Khoi Vu (2007) [10], (6) API 579-N (2000) [11], (7) API 579-L (2000) [11], (8) FITNET (2006) [5].

The applied solutions were:

(a) Kim & Shim [8] (curve 1 in Figure 5):

$$p_Y = \sigma_Y \cdot \frac{t}{R}\left[A \ln\left(\frac{c}{\sqrt{Rt}}\right) + B \right] \qquad (7)$$

(b) R6-Rev. 4 [2] global solution with crack face pressure (curve 2 in Figure 5):

$$p_Y = \sigma_Y \left[\frac{a}{R_i M_{R6}} + \frac{R_i}{R_i + a} \ln\left(\frac{R_o}{R_i + a} \right) \right] \tag{8}$$

(c) BS 7910 [3] no specification (curve 3 in Figure 5):

$$p_Y = \frac{\sigma_Y}{1.2 M_S} \frac{2t}{D} \tag{9}$$

(d) Sattari-Far & Dillström [9] (curve 4 in Figure 5):

$$p_Y = \sqrt{\left(1 - \zeta^{3.11}\right)^{1.9}} \sigma_Y \frac{2t}{D} \tag{10}$$

(e) Staat & Khoi Vu [10] (curve 5 in Figure 5):

$$p_Y = \sigma_Y \cdot \min\left\{ \ln\left(\frac{R_o}{R_i} \right), \left(\frac{R_i}{R_i + a/2} \right) \left[\frac{1}{M_{2S}} \ln\left(\frac{R_i + a}{R_i} \right) + \frac{R_i + a}{R_i} \ldots \right. \right.$$
$$\left. \left. \ldots \ln\left(\frac{R_o}{R_i + a} \right) \right] + \frac{1}{2R_i + a} \left[-2\left(R_i + a\right) + \sqrt{4R_i^2 + 8aR_i + 5a^2} \right] \right\} \tag{11}$$

(f) API 579-N [11] net section collapse (curve 6 in Figure 5):

$$p_Y = \frac{\sigma_Y}{M_{4N}} \frac{2t}{D} \tag{12}$$

(g) API 579-L [11] local collapse (curve 7 in Figure 5):

$$p_Y = \frac{\sigma_Y}{M_{4L}} \frac{2t}{D} \tag{13}$$

(h) FITNET [5] global solution with crack face pressure (curve 8 in Figure 5):

$$p_Y = \sigma_Y \left[\frac{a}{R_i M_{FITNET}} + \frac{R_i}{R_i + a} \ln\left(\frac{R_o}{R_i + a} \right) \right] \tag{14}$$

The Folias factors and other auxiliary functions corresponding to Eqs. (7-14) are given in the Appendix. Unfortunately it cannot be decided which of the solutions is best suited for the purpose of the present analysis although it has to be assumed that the more recently obtained equations are closer to reality than the older ones.

The differences between the yield load solutions are significant with the British Standard BS 7910 solution (3) being a lower bound to all other curves. For common applications this would be conservative. However, in the context of a proof test philosophy conservatism

requires its own definition. In a common analysis conservative means an underestimation of the critical crack size whereas the target of a fracture mechanics analysis of a proof test is the maximum crack size that could have occurred without causing failure. In that case conservative means overestimation! As a consequence upper-bound fracture toughness values have to be used instead of lower-bound toughness for this type of applications. Likewise the yield load solution, if not exact, should provide an upper bound to reality.

With respect to the limit load of structures with semi-elliptical surface cracks in pressurised hollow cylinders it has to be distinguished between global and local yield loads, between solutions obtained for von Mises and Tresca yield criteria, between yield loads considering crack face pressure and those not considering it, and, particularly for older solutions, between plane stress and plane strain solutions [12]. Usually lower bound solutions will be local solutions based on plane stress and Tresca. In contrast upper bound solutions are obtained for plane strain, von Mises and global conditions. The consideration of crack face pressure lowers the yield load compared to analyses which neglect it.

Note that the newer yield load solutions tend to higher values than the older ones, particularly to those of BS 7910. Unfortunately, as can be seen in Figure 5, even they do not give identical results with respect to the crack depth (a/t; t = wall thickness) dependency for the a/c ratios investigated. The Staat & Khoi Vu equation (curve 5) leads to the highest yield loads for short cracks, but this is not the case for longer cracks, the Kim & Shim approach (curve 1) gives high yield loads for $a/t < 0.7$, the FITNET (curve 8) and the R6-Rev. 4 (curve 2) solutions yield almost identical values, the Sattari-Far & Dillström equation (curve 4) shows lower limit loads than the other equations for short cracks, but higher limit loads for long cracks. Finally, both API criteria (curves 6 and 7) give nearly identical results for $a/c < 0.6$.

For the further analysis the global solution of the FITNET compendium was applied to the boost pressure of 65.5 MPa whilst its local solution was used for the subsequent residual lifetime analysis (see Section 3.3). The SAF 2507 steel was very ductile because of which the potential tube failure was predicted as plastic collapse according to the L_r^{max} criterion of Eq. (5). Since the maximum crack size at failure also depends on the crack geometry a/c the analysis was carried out for various combinations of crack depths, a, and crack lengths at surface, 2c. The result is shown in Figure 6 where the grey area marks a-c-combinations for which failure was predicted. The limit curve for crack dimensions which would just survive (or just fail) the test is shown as fat dashed line. The subsequent residual lifetime analysis has to be carried out for a number of different initial crack depths and lengths according to this line.

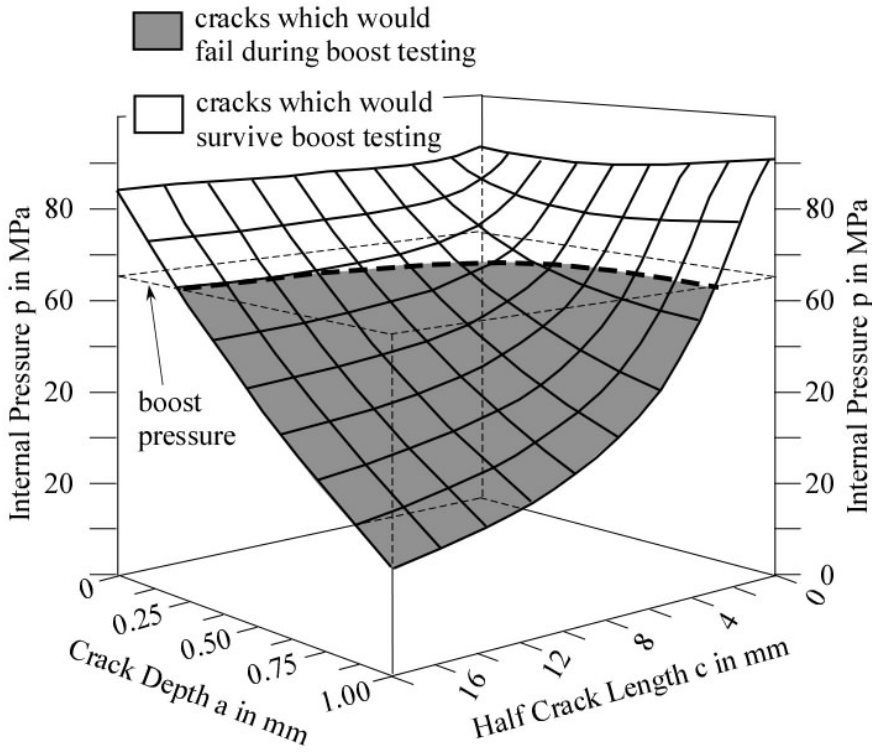

Figure 6: Crack depth (a) – half crack length (c) combinations for which failure by plastic collapse was predicted by using Eqs. (5) and (14) (grey area) or excluded (white area). The fat dashed line marks all combinations of a and c for which the tube would just survive (or just fail) the proof test.

2.3 Fatigue Crack Extension

As mentioned above, empirical evidence showed that the ovality, here determined by the relation $(D_{max}-D_{min})/D$ (definition based on DNV OS F101) of the damaged tube was 0.55. During boost loading the tubes were re-rounded this way causing residual stresses which had to be considered in the fatigue crack extension analysis. Therefore, the complete deformation history including ovalization, re-rounding and relaxation during the shutdowns was modelled by finite elements using the program ANSYS 10.0. The calculations were performed for large deformations and isotropic hardening. Due to symmetry conditions, only one half of the cross-section had to be modelled. The section was idealized by plane strain elements with mid-side nodes.

It was found that ovalization caused stresses up to 620 MPa. The maximum values were obtained in the centre of the wall at the 6 o'clock, 9 o'clock and 12 o'clock positions. At the 9 o'clock position, high stresses were also obtained at the inner surface of the wall. The subsequent re-rounding left high plastic deformations in the pipe wall the relaxation of which was also simulated. The first principal stresses after relaxation are shown in Figure 7. For the subsequent analysis these stresses had to be split into primary and secondary (residual) components. This was done by subtracting the known secondary stresses from the overall load case.

For determining stress intensity factors according to

$$K_I = \left[\sum_{j=0}^{3} \sigma_j \cdot i_j \cdot \left(\frac{a}{t} \right)^j \right] \cdot \sqrt{\pi a} \tag{15}$$

with the coefficients i_j being given in [14] the residual hoop stress profile was approximated by a polynomial

$$\sigma = \sum_{j=0}^{3} \sigma_j \cdot \left(\frac{x}{t} \right)^j \tag{16}$$

which was solved as σ (in MPa) = $-122.73 - 2927.5 \left(\frac{x}{t} \right) + 14984 \left(\frac{x}{t} \right)^2 - 14040 \left(\frac{x}{t} \right)^3$.

for the 9 o'clock position. The distance x is the path from the inner to the outer wall surface and t is the wall thickness such that x/t = 0 marks the position at the inner and x/t = 1 the position at the outer surface of the tube.

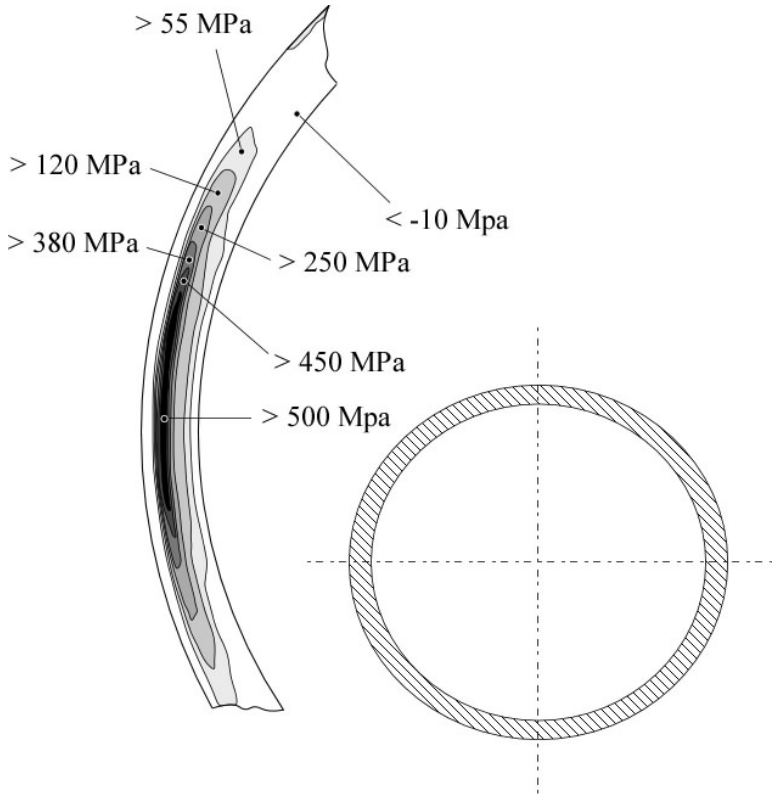

Figure 7: Distribution of mode I residual stresses at the 9 o'clock position after ovalization, re-rounding and relaxation.

The determination of the crack size corresponding to final failure during service loading was carried out using the method described in Section 3.2. However the conditions for conservatism were reversed again, i.e., the analysis had to be performed for a yield load

solution which underestimated reality. As mentioned above, in the present case the local yield load of the FITNET compendium was chosen:

$$p_Y = \frac{\sigma_Y}{c + s_4\left(1 - a/t\right)}\left[s_4\left(1 - a/t\right)\ln\left(\frac{R_a}{R_i}\right) + c\,\frac{R_i}{R_i + a}\ln\left(\frac{R_a}{R_i + a}\right)\right] \tag{17}$$

Furthermore, in order to consider the effect of combined primary and secondary loading on the critical crack size Eq. (1) had to be modified by an interaction term V which describes both ligament yielding and relaxation effects caused by the secondary stresses:

$$K_r = \left(K^p + V \cdot K^s\right) \Big/ K_{mat} \tag{18}$$

No detailed description on the analytical determination of V shall be given here since this can be found in various sources, e.g. [2-6].

The determination of the fatigue crack propagation up to finale failure was based on a Paris type equation

$$\frac{da}{dN} = C \cdot \Delta K^n . \tag{19}$$

In order to take into account crack closure effects this was extended in the NASGRO approach [13] to

$$\frac{da}{dN} = \begin{cases} \dfrac{C \cdot \left(\dfrac{1-f}{1-R}\Delta K\right)^n \cdot \left(1 - \dfrac{\Delta K_{th}}{\Delta K}\right)^p}{\left(1 - \dfrac{K_{max}}{K_c}\right)^q} & \text{for } \Delta K > \Delta K_{th} \\ 0\,\text{mm} & \text{for } \Delta K \le \Delta K_{th} \end{cases} \tag{20}$$

with f being an analytical crack closure correction function defined by

$$f = \begin{cases} \max\left(R, \sum_{i=0}^{3} A_i \cdot R^i\right) & \text{if } R \ge 0 \\ A_0 + A_1 \cdot R & \text{if } R < 0 \end{cases} \tag{21}$$

with

$$A_0 = (0.825 - 0.34\alpha + 0.05\alpha^2) \cdot \left[\cos\left(\frac{\pi}{2} \cdot \frac{\sigma_{max}}{\sigma_Y}\right)\right]^{\frac{1}{\alpha}}, \tag{22}$$

$$A_1 = (0.415 - 0.071\alpha) \cdot \frac{\sigma_{max}}{\sigma_Y}, \tag{23}$$

$$A_2 = 1 - A_0 - A_1 - A_3, \tag{24}$$

and $$A_3 = 2A_0 + A_1 - 1. \quad (25)$$

The fit parameters p and q were chosen as p = 0.25 and q = 0, the constraint value as α = 2.5 and the stress ratio as $\sigma_{max}/\sigma_Y = 0.3$ such as recommended for steels in [13].

The fatigue crack propagation analysis was performed stepwise such as illustrated in Figure 8 starting with various maximum crack depth-crack length-combinations which even could have survived boost loading. What is important in such analyses is the independent treatment of the depth and length growth of the crack. The assumption of a constant a/c ratio would lead to a severe error in residual lifetime. Note that the end-of-life-analysis described above is incorporated in each cycle of the iterative fatigue crack propagation analysis.

The effect of the residual stresses on fatigue crack propagation is different to those on final failure as it was described above. The fatigue crack is driven by the cyclic stress intensity factor ΔK which is not affected by the residual stresses. However, the latter shift the K_{min} and K_{max} in each loading cycle by the same absolute value this way changing the R ratio of the loading. In order to cover this effect the analysis was based on the NASGRO approach of Eqs. (18)-(23) because this allows for variable R ratio analysis.

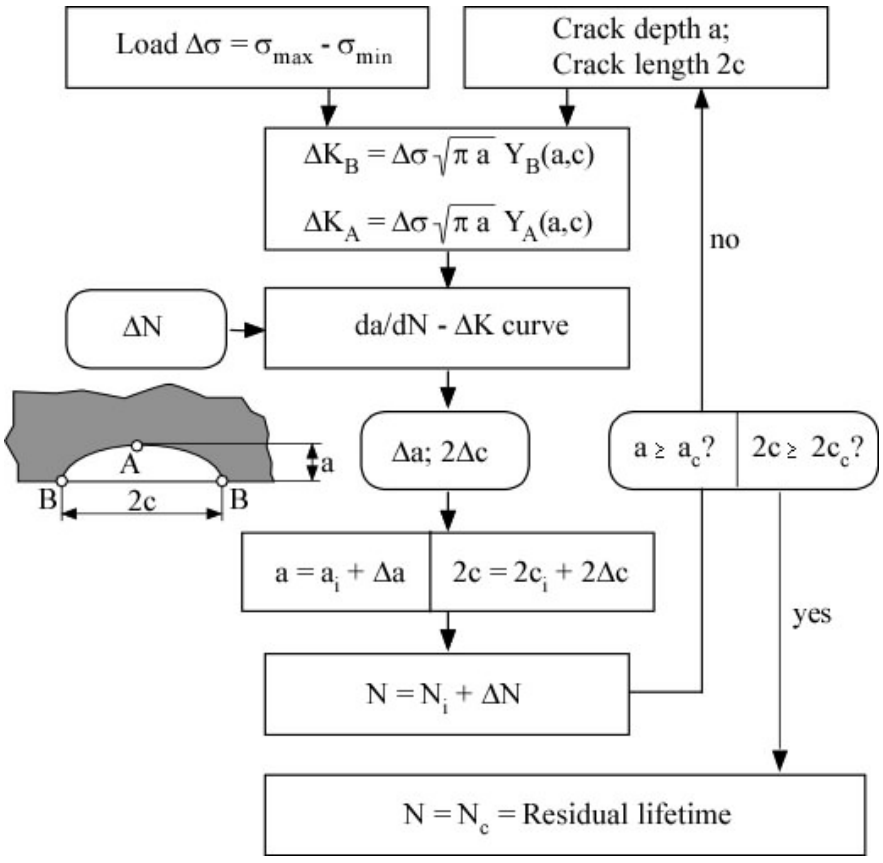

Figure 8: Scheme of the determination of residual lifetime in a fatigue crack extension analysis.

2.4 Residual Lifetime: Results and Discussion

The results of analyses for three possible maximum crack sizes (a = 0.44 mm, c = 4.4 mm / a = 0.67 mm, c = 3.35 mm / a = 0.86 mm, c = 3.2 mm) after boost loading are illustrated in Figure 9. Note that the calculations were terminated for the first two cases after 5.000 loading cycles without failure. However, the last case yielded final failure by plastic collapse after only 1820 loading cycles. This example was chosen such that the minimum residual lifetime for all possible a-c-combinations after proof testing was predicted. Since no information on the initial crack geometry in the installed umbilical was available the lowest value of 1820 cycles had to be chosen as a basis for any decision-making.

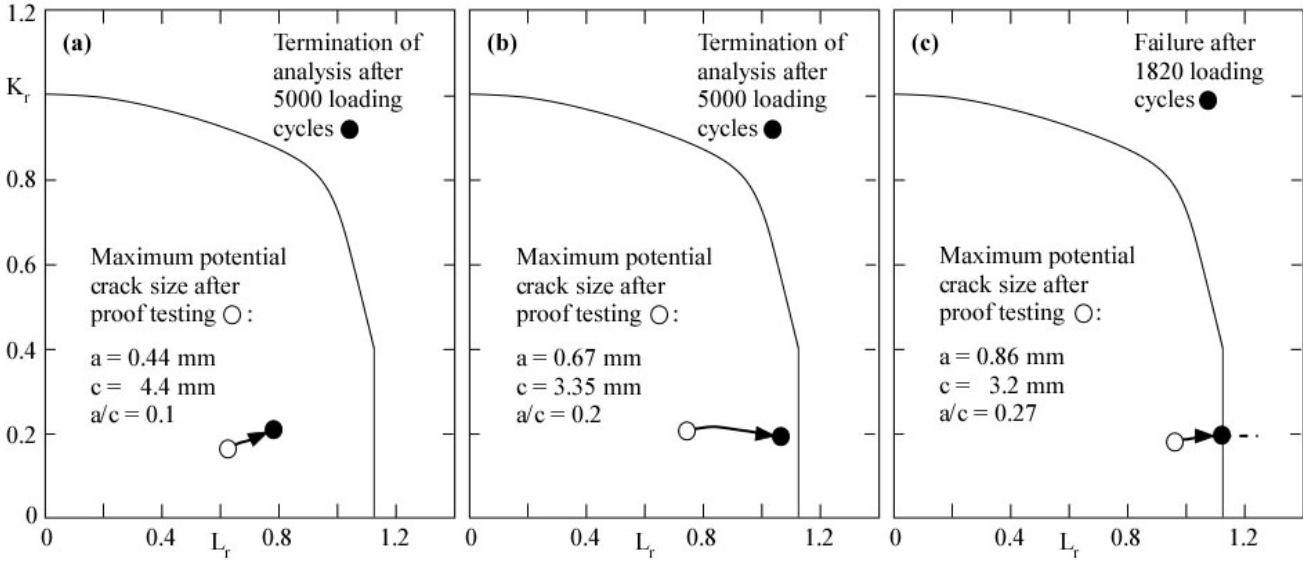

Figure 9: Final results: The analyses were terminated after 5000 loading cycles for crack dimensions of a = 0.44 mm (a) and c = 4.4 mm and of a = 0.67 mm and c = 3.35 mm (b). No failure was predicted up to that time. The third crack (a = 0.86 mm, c = 3.2 mm) (c) was predicted to grow up to its critical size within only 1820 loading cycles.

Note that this is a worst case prediction, i.e., it is based on a number of pessimistic assumptions:

(a) The tube under consideration was largely damaged before and/or during boost loading. Little increase in pressure would have yielded failure already during this action.

(b) The applied yield load solutions for both, maximum crack size at boost loading and final failure are probably conservative. However, even moderate changes in the yield load could be of tremendous effect on the final result.

Therefore, a throughout validation of the recently proposed yield load solutions and, perhaps, the development of further improved solutions is a key issue for reducing the inherent conservatism of fracture mechanics analyses in conjunction with any proof test philosophy.

An additional factor which, however, did not affect the present analyses is the use of upper and lower bound fracture toughness values. By now statistical approaches are only available

for the lower bound. In order to perform meaningful statistical assessments in conjunction with proof tests also a method for upper bound statistics should be developed.

An alternative approach to reduce the conservatism of the analyses is to provide further information, e.g, on the crack geometry range a/c to be expected after ovalization and re-rounding of similar components. And of cause any application of non-destructive inspection would have a most beneficial effect.

3. SUMMARY AND CONCLUSION

The residual lifetime and fitness for service of a pre-damaged tube of a subsea umbilical was determined. The tube had experienced large ovalisation and re-rounding by applying a boost pressure prior to service. The aim of this paper was to describe and to critically discuss the methodology of the fracture mechanics analysis required in addition to leak tightness testing. Special emphasis was put on the reversal of conservatism between the two steps:

(a) Determination of the maximum crack size in the component which just would not have caused component failure under the boost loading applied for re-rounding the tubes, and

(b) Prediction of the residual lifetime of the component under in-service loading assuming the existence of the maximum possible crack size of step (a).

A number of yield load solutions for axial cracks in pressurised hollow cylinders was applied which yielded quite different results. The fatigue crack extension analyses were performed for various crack depth-crack length combinations which just would have survived the boost pressure. For both the simulation of crack propagation under service load and the prediction of the end-of-life state residual stresses due to the pre-history of the tube were considered. The information on these stresses was provided by finite element simulation.

LITERATURE

[1] Zerbst, U. Schwalbe, K.-H. and Ainsworth, R.A. (2003): An overview of failure assessment methods in codes and standards. In: Ainsworth, R.A. and Schwalbe, K.-H. (eds.) (2003): Practical Failure Assessment Methods. Comprehensive Structural Integrity (CSI), Elsevier, Amsterdam et al., Vol. 7., Chapter 7.01, pp. 4-48.

[2] R6, Revision 4 (2000): Assessment of the Integrity of Structures Containing Defects. British Energy Generation Ltd (BEGL), Barnwood, Gloucester.

[3] BS 7910 (2005): Guide on Methods for Assessing the Acceptability of Flaws in Metallic Structures. British Standard Institution (BSI), London

[4] SINTAP (1999): Structural Integrity Assessment Procedure. Final Revision. EU-Project BE 95-1462. Brite Euram Programme, Brussels.

[5] Kocak, M., Webster, S., Janosch, J.J., Ainsworth, R.A. and Koers, R. (2006): Fitness for Service Procedure (FITNET), Final Draft 7.

[6] Zerbst, U., Schödel, M., Webster, S. und Ainsworth, R.A. (2007): Fitness-for-Service Fracture Assessment of Structures Containing Cracks. A Workbook based on the European SINTAP/FITNET Procedure. Elsevier-Verl., Amsterdam, Bosten, Heidelberg, London, New York, Oxford, Paris, San Diego, San Francisco, Singapore, Sydney Sydney und Tokio.

[7] RiserTec Ltd. (2006): Fracture Assessment of Umbilical cores.

[8] Kim, Y.-J. and Shim, D.-J. (2005): Relevance of plastic limit loads to reference stress approach for surface cracked cylinder problems. Int. J. Pressure Vessel and Piping 82, pp. 687-699.

[9] Sattari-Far, I. und Dillström, P. (2004): Limit load solutions for surface cracks in plates and cylinders using finite element analysis. Int. J. Pressure Vessel Piping 81, pp. 57-66.

[10] Staat, M. and Vu, D.K. (2007): Limit analysis of flaws in pressurized pipes and cylindrical vessels. Part I: Axial defects. Engng. Fracture Mech. 74, 431-450.

[11] API 579 (2000): Recommended Practice for Fitness for Service. American Petroleum Institute (API), Washington.

[12] Miller, A.G. (1988): Review of limit loads of structures containing defects. Int. J. Pressure Vessel & Piping 32, pp. 197-327.

[13] NASGRO (2007): Fatigue Crack Growth Computor Program „NASGRO“, Version 5.1. NASA, L.B. Johnson Space Centre, Houston, Texas. Reference Manual JSC-22267B.

[14] RCC-MR Code (2007): Design and Construction Rules for Mechanical Components of FBR Nuclear Islands and High Temperature Applications, Appendix A 16. AFCEN.

APPENDIX: Folias factors and other auxiliary functions corresponding to Eqs. (7-14)

BS 7910:

$$M_S = \frac{1-\frac{a/t}{M_T}}{1-a/t} \tag{A1}$$

$$M_T = \sqrt{1+1.6\frac{c^2}{R_i t}} \tag{A2}$$

R6-Rev. 4:

$$M_{R6}(a,c,t) = \sqrt{1+1.61\frac{a}{(a/c)^2 R_i}} \tag{A3}$$

FITNET:

$$M_{FITNET} = \sqrt{1+1.05\frac{a}{(a/c)^2 R_i}} \tag{A4}$$

$$s_4 = \frac{ac}{R_i M_{FITNET}\left[\ln\left(\frac{R_a}{R_i}\right)-\frac{R_i}{R_i+a}\ln\left(\frac{R_a}{R_i+a}\right)\right]-a} \tag{A5}$$

Sattari-Far & Dillström:

$$\zeta = \begin{cases} \dfrac{ac}{t(c+t)} & \text{for } 2W > 2(c+t) \\ \dfrac{ac}{tW} & \text{for } 2W < 2(c+t) \end{cases} \tag{A6}$$

Staat & Khoi Vu:

$$M_{2S} = \sqrt{1+1.25\frac{c^2}{(R_i+a)a}} \tag{A7}$$

Kim & Shim:

$$A = \left[-1 + 0.847 \tanh\left(0.352 \frac{R_m}{t} \right) \right] a/t + 0.006 \tag{A8}$$

$$B = \left[-1 + 0.751 \tanh\left(0.256 \frac{R_m}{t} \right) \right] a/t + 2 - 0.98 \tanh\left(0.312 \frac{R_m}{t} \right) \tag{A9}$$

API 597-L (local collapse):

$$\lambda = \frac{1.818c}{\sqrt{R_i t}} \tag{A10}$$

$$M_{tAPIL} = \sqrt{\frac{1.02 + 0.4411\lambda^2 + 0.006124\lambda^4}{1.0 + 0.02642\lambda^2 + 1.533 \cdot 10^{-6}\lambda^4}} \tag{A11}$$

$$M_{4L} = \frac{1 - C(a/t) \cdot M_{tAPIL}^{-1}}{1 - C(a/t)} \tag{A12}$$

$$C = 0.85$$

API 597-L (net section collapse)

$$\lambda_a = \frac{1.818c}{\sqrt{R_i a}} \tag{A13}$$

$$M_{tAPINS} = \sqrt{\frac{1.02 + 0.4411\lambda_a^{\,2} + 0.006124\lambda_a^{\,4}}{1.0 + 0.02642\lambda_a^{\,2} + 1.533 \cdot 10^{-6}\lambda_a^{\,4}}} \tag{A14}$$

$$M_{4N} = \frac{1}{1 - (a/t) + (a/t) \cdot M_{tAPINS}^{-1}} \tag{A15}$$

NOMENCLATURE

a	Crack depth
c	Half crack length in surface direction
C, m	Fitting parameters of the Paris range of the da/dN-ΔK curve
da/dN	Fatigue crack propagation rate
D	Mean diameter of the tube; $D = R_o + R_i = 2R$
D_{max}	Larger diameter of the ovalized tube
D_{min}	Smaller diameter of the ovalized tube
E	Modulus of elasticity (Young's modulus)
F	Load (general term)
F_Y	Net section yield load (general term)
K	Stress intensity factor (K factor)
K_{mat}	General term of fracture toughness expressed in terms of the K factor
K_r	Ordinate of the Failure Assessment Diagram (FAD) ($= K/K_{mat}$)
K^p	Stress intensity factor for primary loading
K^s	Stress intensity factor for secondary loading
K_I	Mode I stress intensity factor
L_r	Ligament yielding parameter ($= F/F_Y = \sigma_{ref}/\sigma_Y$), abscissa of the FAD diagram
L_r^{max}	Plastic collapse limit L_r value
N	Number of loading cycles
N_c	Critical number of loading cycles at fracture
p	Internal pressure
p_{max}	Upper service pressure
p_{min}	Lower service pressure; static head pressure
p_{boost}	Boost pressure applied for re-rounding the tubes
p_Y	Yield internal pressure

R	Mean radius of the tube; $R = 0.5\ (R_o + R_i) = 0.5\ D$
R_m	Uniaxial tensile strength
R_i, R_o, $\bar{R}$	Inner, outer and mean radius of hollow cylinders
R	Stress ratio in fatigue crack propagation, $R = K_{min}/K_{max}$
t	Wall thickness of the component
V	Correction factor for primary and secondary stresses interaction
x	Distance from the outer wall surface
α	Constraint parameter (Eqs. 21 and 22)
Δa, Δc	Fatigue crack propagation in depth and surface directions referring to ΔN loading cycles (Figure 8)
ΔK	Stress intensity factor range, $\Delta K = K_{max} - K_{min}$
ΔK_{eff}	Crack closure corrected effective ΔK
ΔK_{th}	Threshold value of ΔK below which there is no crack propagation
ε_{ref}	Reference strain (Figure 4)
σ	Stress
σ_j	Polynomial coefficients for fitting the stress distribution (Eq. 16)
σ_{max}	Upper stress; cyclic loading (Eq. 22)
σ_{ref}	Net section reference stress ($= L_r \cdot \sigma_Y$)
σ_Y	Yield strength (for materials with Lüders' plateau $R_{p0.2}$)